https://doi.org/10.20965/jaciii.2017.p0387

Paper:

Generalized Potential Function-Based Cooperative Current-Sharing Control for High-Power Parallel Charging Systems

Hongtao Liao, Jun Peng, Yanhui Zhou, Zhiwu Huang, and Feng Zhou

School of Information Science and Engineering, Central South University
Changsha 410075, China
E-mail: lht@csrzelc.com, {pengj, zyh5276, hzw}@csu.edu.cn, zhoufengcsu@qq.com
[Received July 5, 2016; accepted November 19, 2016]

In this paper, a new decentralized gradient-based cooperative control method is proposed to achieve current sharing for parallel chargers in energy storage-type light rail vehicle systems. By employing a generalized artificial potential function to characterize the interaction rule for subchargers, the current-sharing control problem is converted into an optimization problem. Based on the gradient of the potential function, a decentralized gradient cooperative control law is derived. A general saturation function is introduced in the proposed control to guarantee the boundedness of the control output. The stability of the closed-loop system under the proposed decentralized gradient control is proven with the aid of a Lyapunov function. Simulation results are provided to verify the feasibility and validity of the proposed distributed current-sharing control method.

Keywords: current-sharing, cooperative control, parallel charging

1. Introduction

Supercapacitors have many advantages over energy storage batteries, such as large capacitance, high power density, quick charge/discharge with instantaneous large current, and long cycle life. As an emerging energy storage component, supercapacitors have been adopted as the main power supply for energy storage-type light rail vehicles. With this technology, a traction power grid is no longer needed to construct a light rail system, and a regenerative braking system can be designed to save energy.

In order to keep light rail vehicles running at high efficiency, supercapacitors need to be fully charged during each parking period at the platform, which requires the charging system to supply a large enough current to speed up the process. A single charger is difficult and expensive to obtain, thus several chargers can be connected in parallel to boost the system's capacity and form redundancy [1, 2]. However, this may also lead to a current imbalance problem among chargers [3, 4].

Current imbalance is mainly caused by the intrinsic difference between the parameters of each component in the circuit, especially the difference in each supercapacitor's capacitance, which is nonlinear and affected by input voltage. If the charging current is not balanced, the charger with higher current has to bear a larger output power, which may lead to high thermal stress and higher risk of system breakdown during prolonged operation [4]. Thus, current imbalance may degrade the performance and reliability of the whole charging system. It is necessary to adopt an effective current-sharing control strategy to balance the output current of charging systems.

There are several solutions to current-sharing problems, such as the droop control method [5], master-slave method [6, 7], central current-sharing control method [7], and distributed current sharing control method [8]. The droop control method achieves current balance by tuning the output impedance. This method is simple and has been widely used in parallel charging systems with small capacity. However, for large capacity systems or large variance load systems, this method ceases to be effective and suitable [9]. The master-slave method arbitrarily designates one power module as the master module while the rest are designated as slave modules, which follow the master module's allocation current [6, 7]. The central current-sharing control method contains a central controller to compute each module's output current according to the total load current. The common disadvantage of the master-slave method and the central current-sharing control method is that a faulty master module or a central controller can cause the whole system to collapse, thus decreasing the system's reliability.

In the distributed control method, each parallel charger has its own autonomous controller, which communicates and exchanges state information with other chargers. It can be easily expanded to increase the system's charging power and form redundancy, to improve the system's reliability. The failure of one charger will not cause the collapse of the whole system. Distributed consensus and cooperative control were recently applied to current-sharing control [8], where the current-sharing problem was converted into a current consensus-tracking problem of nonlinear and non-identical multi-agent systems. The adja-

cent chargers interacted with each other and exchanged state information on the charging current, which allowed the cooperative current-sharing objective to be achieved.

However, in practical applications, two aspects of the cooperative control law [8] need to be improved: the disturbance rejection and convergence rate performance. On the one hand, the charger is intrinsically nonlinear because of the principles of the buck DC/DC circuit as well as the features of the supercapacitor. The charger is also inevitably affected by the disturbances mentioned above. Current consensus-tracking control is essentially a proportional control method for each agent [8], which makes it hard to address the problems of nonlinearity and disturbances.

On the other hand, the distributed control law is based on the state difference between neighbors, which is actually a gradient of a special potential function formed by the square of the state difference between neighboring agents [8]. The potential function is associated with the convergence rate, but the omitted potential function in [8] is fixed and cannot be changed, which means that convergence rate performance cannot be improved by adopting more suitable potential functions. To solve these problems, a generalized artificial potential function (APF)-based decentralized gradient control would be a good option.

The APF-based gradient nonlinear control is a real-time optimization tool, whose purpose is to autonomously find an optimal point for the potential function, while maintaining the stability and boundedness of signals. Potential functions have been widely used for multi-agent coordination [10–12]. A potential function is created to contain the scalar signal to be tracked as well as the interaction rules for a group of agents. The parallel current charging process can be divided into two parts. One is the sub-chargers' current synchronization and the other is target current tracking. Thus, the current-sharing objective can be treated as a potential function optimization problem. By minimizing the potential function, target tracking and current synchronization can be achieved simultaneously. A generalized APF provides flexibility for convergence rate improvements, and the nonlinear decentralized gradient control is applied to address the problems of nonlinearity and disturbances.

In this paper, we seek to solve the current imbalance problem of supercapacitor chargers by gradient based optimization based on a generalized potential function, while taking into account the control input constraints. The main contribution of the paper can be summarized as follows.

First, by introducing a potential function, the current-sharing control problem of the charging system for energy storage-type light rail vehicles is converted into an optimization problem.

Second, an APF-based decentralized gradient control is developed by treating the charging system as a decentralized nonlinear multi-agent system. A potential function is created to characterize the interaction rule for the group, which is composed of two parts. The agent-target function contains the scalar signal to be tracked, which directs the group's behavior for target tracking. The agent-agent function forms the interconnection part which makes the agent synchronize its state during the whole process. Third, since the control signal of the charger is the duty ratio, which is physically constrained between 0 and 1, a general saturation function is added into the proposed control to satisfy input constraints. Fourth, the overall system stability is rigorously proven using the Lyapunov method.

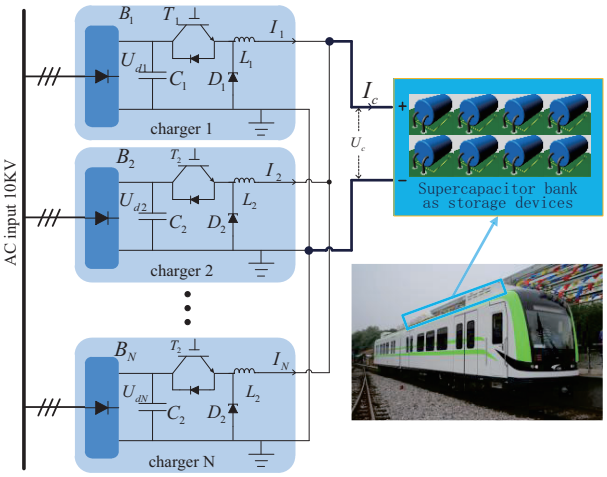

Fig. 1. Schematic diagram of main circuit of charging system for energy storagetype light rail.

The rest of this paper is organized as follows. Section 2 discusses the current-sharing problem, charging system analysis, and modeling. Section 3 elaborates the current-sharing strategy using the APF-based decentralized gradient control, followed by stability analysis. The simulation results of current-sharing cases are given in Section 4. Finally, Section 5 presents the conclusions.

2. Charging System Analysis and Modeling

2.1. Charging System Composition and Problem Formulation

As shown in **Fig. 1**, the charging system for the energy storage-type light rail vehicle is composed of a 10 kV AC supply grid, a 10 kV/900 V AC converter, and four parallel connected chargers, which can exchange state information by communicating with each other. We need the charger to have an output current of 1800 A, which means an equal average output current of 450 A for each charger. The charging process is completed when the supercapacitor's terminal voltage reaches 900 V. Because of the intrinsic differences between the parameters of components in the circuit as well as disturbances, the output current of each charger is difficult to balance. Therefore, the purpose of this study is to design a control law to balance the output current of each charger.

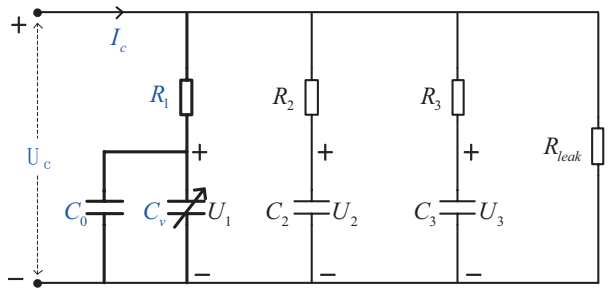

Fig. 2. Equivalent three branches RC circuit model of the supercapacitor.

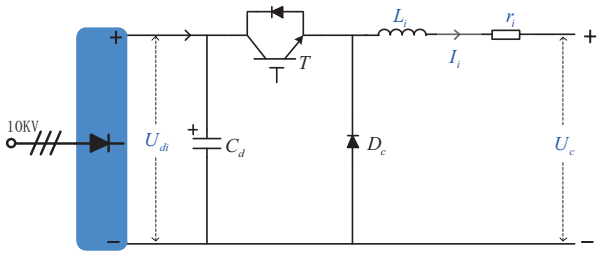

Fig. 3. Buck circuit for each charger subsystem.

2.2. Super Capacitor Modeling

As the storage device for the energy storage light rail vehicle system, the supercapacitor is the charging target. It is intrinsically nonlinear [13] and its capacitance C_{sc} rises with increasing voltage. Electric charge redistribution occurs when the charging process ends; a leakage current also exists. There are several methods for supercapacitor modeling, but the Three Branches equivalent modeling method is widely used because of its accuracy and practicability. As **Fig. 2** shows, a supercapacitor can be divided into three capacitor-resistor branches and a leakage resistor branch. Each branch has its own time constant, which varies widely from each other. The first branch or immediate branch is composed of a resistor R_1, a constant capacitor C_0, and a variable term C_v proportional to the terminal voltage $C_v \cdot U_c$. Its time constant is in seconds. The second branch or delay branch includes a capacitor C_2 and a resistor R_2, and its time constant is in minutes. The third branch or long-term branch, includes a capacitor C_3 and a resistor R_3, and a time constant to the 10 min level. According to the time constant, the first branch reflects almost all behaviors in a charging process, so the capacitance of the first branch can be equally used as the capacitance of the supercapacitor, denoted as $C_{cs} = C_0 + C_v U_c$, which shows that the capacitance is linear with its terminal voltage.

The dynamics then can be described as

$$\dot{U}_c = \frac{I_c}{C_{sc}} = \frac{1}{C_0 + C_v U_c} \sum_{i=1}^{4} I_i. \quad \ldots\ldots\ldots \quad (1)$$

2.3. Charger Modeling

Figure 3 specifically depicts one charger from the diagram of the charging system in **Fig. 2**. It can be seen that the charger mainly consists of a chopper buck DC/DC circuit and a three-phase bridge rectifier circuit. U_{di} is the input DC voltage, U_c is the supercapacitor's terminal voltage, I_i is the output current of the i-th charger, L_i is the inductor, r_i is the equivalent resistance, and D_i is the insulated gate bipolar transistor (IGBT) duty ratio. According to Kirchhoff's voltage law, the current dynamics can be obtained as follows:

$$\dot{I}_i = -\frac{r_i}{L_i} I_i - \frac{U_c}{L_i} + \frac{U_{d_i}}{L_i} \quad \ldots\ldots\ldots\ldots \quad (2)$$

$$\dot{I}_i = -\frac{r_i}{L_i} I_i - \frac{U_c}{L_i}, \quad \ldots\ldots\ldots\ldots \quad (3)$$

where Eqs. (2) and (3) represent the conditions when IGBT is ON and OFF, respectively. To obtain uniform dynamics for all times, there are several modeling methods available, among which the average value modeling method is the most practical and effective [14, 15]. To adopt this method, we can obtain uniform current dynamics as

$$\begin{aligned}
\dot{I}_i &= \left(-\frac{r_i}{L_i} I_i - \frac{1}{L_i} U_c + \frac{U_{d_i}}{L_i} \right) * D_i \\
&\quad + \left(-\frac{r_i}{L_i} I_i - \frac{1}{L_i} U_c \right) * (1 - D_i) \\
&= -\frac{r_i}{L_i} I_i - \frac{1}{L_i} U_c + \frac{U_{d_i}}{L_i} D_i \\
&= -\frac{r_i}{L_i} I_i - \frac{1}{L_i} U_c + \frac{1}{L_i} u_i \quad \ldots\ldots\ldots \quad (4)
\end{aligned}$$

where $u_i = U_{d_i} D_i$ represents the control input to facilitate later analysis. $D_i \in [0,1]$ determines $u_i \in [0, U_{d_i}]$, which is a constraint for the system that will also be discussed later. From Eqs. (1) and (4), we can see that the charging model is nonlinear and has a coupling relationship with each other.

We can convert the i-th charger dynamic model into a more general form, described as

$$\begin{aligned}
\dot{x}_i &= f_i(x_i) + g_i(x_i) u_i \\
y_i &= h_i(x_i), \quad \ldots\ldots\ldots\ldots\ldots\ldots \quad (5)
\end{aligned}$$

where $i = 1,2,3,4$, $x_i = I_i \in \mathbb{R}$ is the i-th charger's state, u_i is the control input as in Eq. (4), system function $f_i(x_i)$ and $g_i(x_i)$ are Lipschitz continuous, and $h_i(x_i)$ is the output of the system, as defined below

$$\begin{aligned}
f_i(x_i) &= -\frac{r_i}{L_i} I_i - \frac{1}{L_i} U_c \\
g_i(x_i) &= \frac{1}{L_i} \\
h_i(x_i) &= I_i. \quad \ldots\ldots\ldots\ldots\ldots\ldots \quad (6)
\end{aligned}$$

Our objective is to design a control law $u_i(t)$ to overcome the system's nonlinearity, coupling restriction, and unpredictable disturbances, thus balancing the current of

every charger. Described in mathematical form we have

$$\lim_{x\to\infty} |x_i - x_t| = 0, \quad \ldots \quad (7)$$

where x_t is the target current trajectory. x_t should be predetermined by $x_t = I_c/n$, where I_c represents the total current of subchargers.

3. Current-Sharing Strategy Based on the Decentralized Gradient Control

In this section, a generalized potential function is employed to characterize the optimization objective for current sharing with subchargers. A decentralized gradient cooperative control law is designed to serve as a basis. Stability is proven with the aid of a Lyapunov function.

3.1. Preliminary APF-Based Decentralized Gradient Control

The APF-based decentralized gradient control is typically an optimization problem of the potential function. The optimal value is found literally from the gradient direction of the APF [16–19]. In order to achieve system goals, the design of the APF becomes very critical. The APF must have a global minimum or maximum value, which is the point where the system control objectives are achieved. The gradient of the APF should be easy to calculate analytically and have low computational complexity. To a large extent, the APF determines the convergence rate of the output value. Hence, in order to improve dynamic performance control, the APF should provide some flexibility for design. The nonlinear decentralized gradient control is basically a control method to find the optimal APF value. With some nonlinear control concepts like siding mode, it can address the problems of system nonlinearity and disturbances. With these requirements, the APF-based decentralized gradient control shows excellent control performance.

3.2. Potential Function Design

Consider a multi-agent system consisting of N individuals in n-dimensional Euclidean space. We assume that the i-th agent's motion is governed by the nonlinear model (5). We also assume there is a scalar signal $J_t(x)$ to be tracked by the swarming agents, which has an unknown isolated minimum at $x_t \in \mathbb{R}^n$. Our purpose is to design a control law for each agent such that we can achieve swarm tracking. We consider a potential function composed of several components. The interconnection component puts coordination on the agent based on its neighbor's information, in order to maintain synchronization of the agent's state. In addition, a tracking component containing the scalar signal to be tracked is added to direct the group's behavior for target tracking.

First, consider the potential function for agent to target interaction given by

$$J_{at}(x,x_t) = \sum_{i=1}^{N} J_{it}\left(\|x_i - x_t\|\right), \quad \ldots \quad (8)$$

where J_{it} is the potential between the i-th agent and the target trajectory x_t, which is defined in Eq. (7). J_{it} is assumed to have a minimum at $x_i = x_t$, whose purpose is to track the target for the i-th agent, i.e., target tracking for agents.

Second, consider the potential function for agent to agent interaction given by

$$J_{aa}(x) = \sum_{i=1}^{N-1} \sum_{j=i+1}^{N} J_{ij}\left(\left\|x_i - x_j\right\|\right), \quad \ldots \quad (9)$$

where $J_{ij}(x)$ is the potential between the i-th and the j-th agent, and is assumed to have a minimum at $x_i = x_j$, whose purpose is to achieve synchronization for agents, i.e., state synchronization for agents.

Combining J_{at} and $J_{aa}(x)$ together, the generalized APF for the nonlinear system (5) is formed

$$J(x,x_t) = K_{at}J_{at}(x,x_t) + K_{aa}J_{aa}(x), \quad \ldots \quad (10)$$

where K_{at}, K_{aa} are the weights of the potential components. Obviously, the minimum value of $J(x,x_t)$ appears at $x_i = x_t$ and $x_i = x_j$. If we can design a decentralized controller to minimize the APF, then target tracking and state synchronization can be achieved.

3.3. Control Law and Stability Analysis

In this section, we present a cooperative control law, i.e., the APF-based decentralized gradient nonlinear control. A Lyapunov function is applied to prove the stability of the control law.

1) Cooperative Control Law

First, we introduce a saturation function $\phi(\cdot)$, which satisfies the following assumption

Assumption 1:

(1) $\phi(\cdot)$ is Lipschitz continuous,

(2) $\phi(z) = 0 \Leftrightarrow z = 0$

(3) $z\phi(z) > 0, \forall z \neq 0$

(4) $\phi_{\min} \leq \phi(z) \leq \phi_{\max}, \forall z \in \mathbb{R}$

We assume that $||\dot{x}_t|| \leq \gamma_t$ for some known $\gamma_t > 0$, is a realistic assumption, since $\dot{x}_t$ represents the velocity of a moving target, and velocity is always bounded. With this assumption, let $k_i > 0$, $\beta_i > \gamma_t$, inspired by [17], the controller can be written as

$$\begin{aligned} z_i &= \nabla_{x_i} J(x,x_t) \\ u_i &= \frac{-k_i\phi(z_i) - \beta_i sgn(\phi(z_i)) - f_i(x_i)}{g_i(x_i)}, \quad \ldots \quad (11) \end{aligned}$$

where $sgn(\cdot)$ is the signum function, $\nabla_{x_i} J(x,x_t)$ is the derivative potential function $J(x,x_t)$ at x_i, and $\phi(z)$ is a saturation function with z, which might be a hyperbolic

tangent function as used in [20]. Nonetheless, any function satisfying Assumption 1 would work. From Eq. (6), we can see that $f_i(x_i)$ and $g_i(x_i)$ are bounded. Thus, in Eq. (11), bounded $\nabla_{x_i}J(x,x_t)$ determines a bounded u_i, which meets the practical requirements mentioned in the previous section. The forthcoming subsection will provide detailed proof.

2) Stability Analysis

First, we assume that the following conditions hold for potential function J:

Assumption 2: For $i = 1,\ldots,N$, there exist functions $h_{it} : \mathbb{R}^+ \to \mathbb{R}$ such that

$$\nabla_x J_{it}(\|x\|) = x h_{it}(\|x\|)$$

Assumption 3: There exist unique distances δ_{it} at which we have

$$h_{it}(\delta_{it}) = 0$$

Assumption 4: The potentials $J_{it}(\|x_i - x_j\|)$ are symmetric and satisfy

$$\nabla_{x_i} J_{ij}(\|x_i - x_j\|) = -\nabla_{x_j} J_{ij}(\|x_i - x_j\|)$$

Assumption 5: For $1 \le i,\ j \le N$ there exist functions $g_{ar}^{ij} : \mathbb{R}^+ \to \mathbb{R}$ such that

$$\nabla_x J_{ij}(\|x\|) = x\, g_{ar}^{ij}(\|x\|)$$

Assumption 6: There exist unique distances δ_{ij} at which we have

$$g_{ar}^{ij}(\|x\|) = \begin{cases} > 0, & \|x\| > \delta_{ij} \\ = 0, & \|x\| = \delta_{ij} \\ < 0, & \|x\| < \delta_{ij}. \end{cases}.$$

The term $g_{ar}^{ij}(\|x\|)$ determines the attraction-repulsion relationship between the individuals. Specifically, it shows attraction when $\|x\| > \delta_{ij}$ and repulsion when $\|x\| < \delta_{ij}$. Hence, $g_{ar}^{ij}(\|x\|)$ can be divided into two parts [17], as

$$g_{ar}^{ij}(\|x\|) = g_a^{ij}(\|x\|) + g_r^{ij}(\|x\|), \quad \ldots\ldots (12)$$

where $g_a^{ij}(\|x\|)$ and $g_r^{ij}(\|x\|)$ represent the attraction and repulsion, respectively. The distance δ_{ij} is the equilibrium point where the attraction and repulsion reach a balance, meaning that $\|x_i - x_j\| = \delta_{ij}$ is the minimum point of the potential function $J_{ij}(\|x_i - x_j\|)$.

Theorem 7: Consider the charging systems Eq. (5) with decentralized control protocols Eq. (11). Under Assumptions 1–6, suppose $k_i > 0$, $\beta_i > \gamma_t$, $\|\dot{x}_t\| < \gamma_t$ for some known $\gamma_t > 0$, the control objective of Eq. (7) can be achieved, i.e., the output current of the parallel chargers can ultimately synchronize to the desired reference current trajectory. That is, the overall closed-loop system is asymptotically cooperative stable.

Proof: With Assumptions 2 and 5, we can obtain the gradient of $J(x,x_t)$ in Eq. (10) with respect to x_i as

$$\begin{aligned}\nabla_{x_i}J(x,x_t) &= K_{at}\cdot\nabla_{x_i}J_{at}(x,x_t) + K_{aa}\cdot\nabla_{x_i}J_{aa}(x)\\ &= K_{at}\cdot\nabla_{x_i}J_{it}(\|x_i - x_t\|) + K_{aa}\\ &\quad\cdot\sum_{j=1,j\neq i}^{N}\nabla_{x_i}J_{ij}(\|x_i - x_j\|)\\ &= K_{at}\cdot(x_i - x_t)h_{it}(\|x_i - x_t\|)\\ &\quad + K_{aa}\cdot\sum_{j=1,j\neq i}^{N}(x_i - x_j)g_{ar}^{ij}(\|x_i - x_j\|),\end{aligned}$$
$$\ldots\ldots\ldots\ldots\ldots (13)$$

and the gradient of $J(x,x_t)$ with respect to x_t as

$$\nabla_{x_t}J(x,x_t) = -K_{at}(x_i - x_t)h_{it}(||x_i - x_t||). \quad \ldots (14)$$

With the transformation of Eq. (13), Eq. (14) can be rewritten as

$$\begin{aligned}\nabla_{x_t}J(x,x_t) &= -\sum_{i=1}^{N}\nabla_{x_i}J(x,x_t)\\ &\quad + K_{aa}\sum_{i=1}^{N}\sum_{j=1,j\neq i}^{N}(x_i - x_j)g_{ar}^{ij}(\|x_i - x_j\|).\end{aligned}$$
$$\ldots\ldots\ldots\ldots\ldots (15)$$

Moreover, since

$$\sum_{i=1}^{N}\sum_{j=1,j\neq i}^{N}(x_i - x_j)g_{ar}^{ij}(\|x_i - x_j\|) = 0, \quad \ldots\ldots (16)$$

which follows from Assumption 4, we obtain

$$\nabla_{x_t}J(x,x_t) = -\sum_{i=1}^{N}\nabla_{x_i}J(x,x_t). \quad \ldots\ldots (17)$$

Now we choose a Lyapunov function candidate as

$$\mathbb{V} = J(x,x_t). \quad \ldots\ldots\ldots\ldots (18)$$

Differentiating Eq. (18) with respect to time t and then substituting Eqs. (5) and (17) into the derivative function $\dot{\mathbb{V}}$, then it follows that

$$\begin{aligned}\dot{\mathbb{V}} &= \sum_{i=1}^{N}\left[\nabla_{x_i}J(x,x_t)\right]^T\dot{x}_i + \left[\nabla_{x_t}J(x,x_t)\right]^T\dot{x}_t\\ &= \sum_{i=1}^{N}\left[\nabla_{x_i}J(x,x_t)\right]^T\left(f_i(x_i) + g_i(x_i)u_i - \dot{x}_t\right). \quad \ldots (19)\end{aligned}$$

Substituting $z_i = \nabla_{x_i}J(x,x_t)$ and u_i into Eq. (19), we get

$$\dot{\mathbb{V}} = \sum_{i=1}^{N} z_i^T\left(-k_i\phi(z_i) - \beta_i sgn(\phi(z_i)) - \dot{x}_t\right). \quad \ldots (20)$$

Since z, $\phi(z)$ and $sgn(z)$ have the same sign componentwise, $||\dot{x}_t|| \le \gamma_t$, $\beta_i > \gamma_t$ as mentioned above, and obvi-

Table 1. Supercapacitor's parameters in simulation.

Parameter	R_1 (mΩ)	C_0 (F)	C_v (F/V)
Value	5.6	92.3	0.0747

Table 2. Four buck circuits' main parameters in simulation.

Buck i	U_{di} (V)	r_i (mΩ)	L_i (mH)
1	1332	3.49	3.15
2	1269	2.98	2.88
3	1288	3.12	2.96
4	1375	3.89	3.01

ously $sgn\,(\phi(z)) = sgn(z)$, so

$$\begin{aligned}\dot{\mathbb{V}} &= \sum_{i=1}^{N}\left(-k_i z_i^T\,\phi(z_i) - \beta_i z_i\, sgn(z_i) - z_i^T \dot{x}_t\right)\\ &= \sum_{i=1}^{N}\left(-k_i z_i^T\,\phi(z_i) - \beta_i\, \|z_i\| - z_i^T \dot{x}_t\right)\\ &\leq -\sum_{i=1}^{N}\left(k_i z_i^T\,\phi(z_i)\right) \leq 0, \quad \ldots\ldots\ldots (21)\end{aligned}$$

to this end, the system is stable.

4. Simulation Examples

4.1. Simulation Cases

In this section, we present three cases to illustrate the feasibility of the APF-based decentralized gradient control for the current-sharing parallel charging system shown in **Fig. 1**. The supercapacitor was modeled as three branches of an RC circuit, as shown in **Fig. 2**, whose main parameters are presented in **Table 1**. Four subchargers are adopted to form the charging system, which means that $N = 4$ in **Fig. 1**. The main parameters of the four buck circuits are given in **Table 2**. We assumed that the initial current is 0 for all the buck circuit simulations. Three different cases are considered below.

Case A: The supercapacitor's charging current is set at 1800 A for the whole charging process. That is to say, each subcharger's output current should be 450 A.

Case B: The whole charging process for each subcharger includes two sequential phases, namely, a fast charging phase with a charging current of 450 A, and a trickle charging phase with a charging current of 100 A.

Case C: On the basis of Case B, a disturbance is added to the buck circuit.

In all cases, the initial current of each subcharger is 0 A. Case A is used to test the feasibility of the APF-based decentralized gradient control technology applied to a current-sharing situation. Case B is used to determine whether the decentralized gradient control can meet the requirements in actual practice. More specifically, when an energy storage-type rail vehicle reaches the platform and the supercapacitor must be charged to 900 V within 30 s for the next trip. The supercapacitor's initial voltage should not be less than 500 V, here, without loss of generality. The initial voltage is set as 500 V. The charger, composed of four parallel subchargers with a charging current of 1800 A, charges the supercapacitor until its voltage reaches 870 V; this is called the fast charging phase. Then, it moves on to the trickle charging phase, where the charging current decreases to 100 A. The charging process is completed when the supercapacitor's voltage reaches 900 V. Case C is used to evaluate the disturbance rejection performance of the APF-based decentralized gradient control applied in current-sharing.

There are four buck circuits and four decentralized gradient controllers in **Fig. 1**. The performance function depicted in Eq. (10) can be formulated in a specific form as

$$\begin{aligned}y = J(x,x_t) &= K_{at}\sum_{i=1}^{4}\frac{1}{2}(x_i - x_t)^2\\ &\quad + K_{aa}\sum_{i=1}^{3}\sum_{j=i+1}^{4}\frac{1}{2}(x_i - x_j)^2. \quad \ldots (22)\end{aligned}$$

The specific final control law u_i and the duty ratio D_i are written as

$$\begin{aligned}z_i &= \nabla_{x_i}J(x,x_t) = K_{at}\sum_{i=1}^{4}(x_i - x_t)\\ &\quad + K_{aa}\sum_{i=1}^{3}\sum_{j=i+1}^{4}(x_i - x_j)\\ u_i &= -L_i k_i \phi(z_i) - L_i\beta_i sgn\,(\phi(z_i))\, r_i I_i + U_c\\ D_i &= \frac{u_i}{U_{di}}, \quad \ldots\ldots\ldots\ldots\ldots (23)\end{aligned}$$

where $r_i, L_i, i = 1,2,3,4$ are given in **Table 2**. The weights of the potential components $K_{at} = 1$, $K_{aa} = 0.1$, the supercapacitor's initial voltage $U_c(0) = 500$, and its initial current $I_i(0) = 0$, $i = 1,2,3,4$ in all cases.

The specific saturation function in Eq. (23) is given as

$$\phi(x) = \begin{cases} a & x > a\\ x & x \in [-a,a]\\ -a & x < -a,\end{cases} \quad \ldots\ldots\ldots (24)$$

where a is a parameter which can characterize the upper and lower bounds of the saturation function. Here, $a = 300$ for all cases in the simulation. In addition, another saturation function with lower bound 0 and upper bound 1 was added to the output control signal duty ratio D_i to ensure that it is strictly confined within $[0,1]$.

4.2. Results and Analysis

In Case A, the current-sharing objective was 450 A, which means that in performance function Eq. (10), the target value $x_t = 450$. The current-sharing curve is plotted in **Fig. 4(a)**, which illustrates that the current quickly achieved synchronization under different initial parameter conditions, and reached the consensus objective when $t = 2$ s. The charger then maintained a constant charging

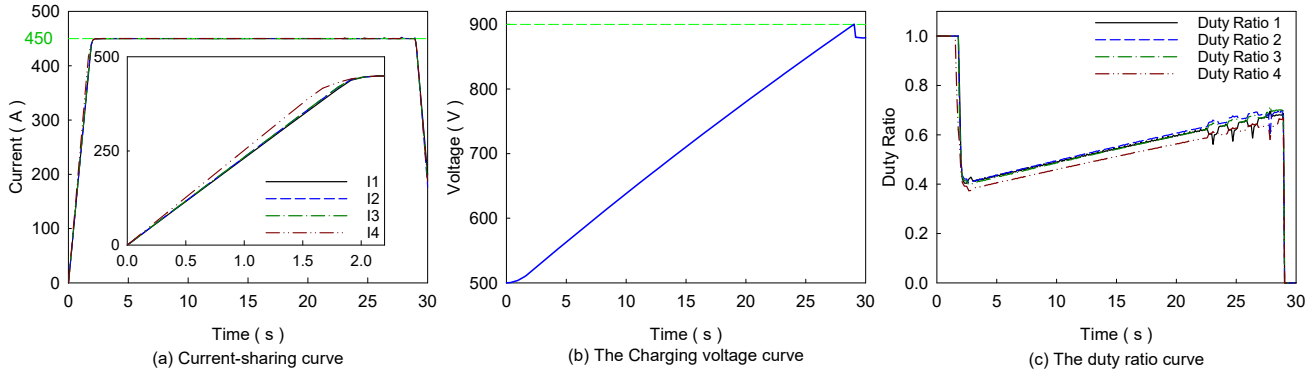

Fig. 4. Current-sharing curve for Case A: under decentralized gradient cooperative control with a target value $x_t = 450$ A until voltage reaches 900 V.

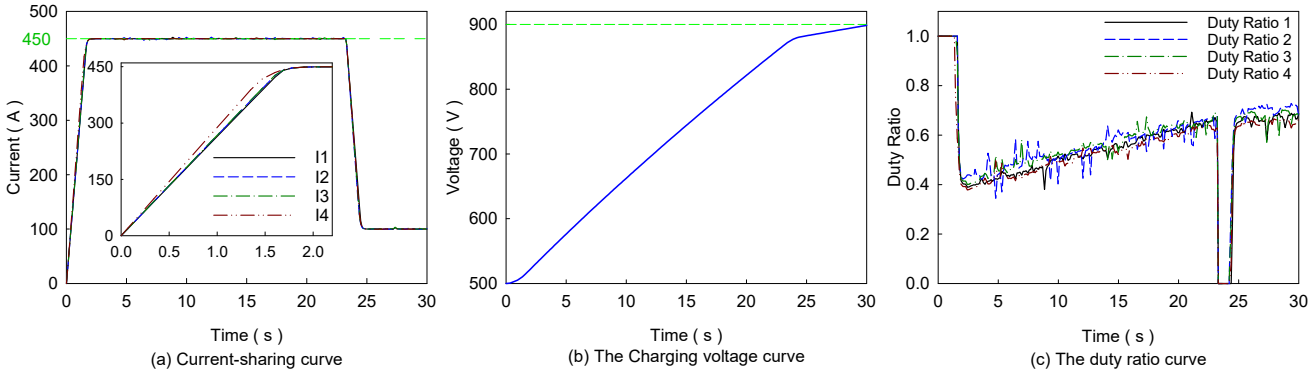

Fig. 5. Current-sharing curve for Case B: under decentralized gradient cooperative control with a fast charging phase ($x_t = 450$ A) until voltage reaches 870 V, and then shifts to the trickle charging phase ($x_t = 100$ A) until voltage reaches 900 V.

current until the supercapacitor's terminal voltage reached 900 V, as shown in **Fig. 4(b)**. This means that the supercapacitor was fully charged, and the control output then dropped to 0 A at a quick response rate, as shown in **Fig. 4(c)**. However, the charging current declined at a lower response rate because of the residual energy stored in the inductor and capacitor of the buck circuit. Moreover, at this point, as shown in **Fig. 4(b)**, the terminal voltage exhibited a sharp drop of approximately 20 V for two reasons. The first was the disappearance of the impedance divider, which was very large under large current. The other reason was the reallocation of the supercapacitor's electric charges. The simulation results show that the APF-based decentralized gradient control can be applied in the current-sharing task of a parallel charging system.

In Case B, the target value $x_t = 450$ was used in the performance function for the fast charging phase, and $x_t = 100$ was used for the trickle charging phase. The current-sharing curve is plotted in **Fig. 5**, which illustrates that under different initial values, the charging current of each subcharger quickly synchronized its value and increased to 450 A from 0 A, when $t = 2$ s. A constant charging current was maintained until the supercapacitor's voltage reached 870 V, which indicated that the fast charging process was over. The charging current then decreased to 100 A as the charging process moved on to the trickle charging phase. The charging process ended when supercapacitor's terminal voltage reached 900 V. As **Fig. 5(b)** shows, the supercapacitor was fully charged when its terminal voltage rose from 500 V to 900 V in less than 30 s. This illustrates that the voltage objective was achieved by adopting the decentralized gradient controller. The control output signal duty ratio is plotted in **Fig. 5(c)**.

A comparison with **Fig. 4(b)** shows that in **Fig. 5(b)**, the supercapacitor was charged to almost exactly 900 V without any excess or decline in voltage. This means that charging tasks cannot be performed effectively and safely using a large current. A better and more practical alternative is to use a large charging current during the first stage for a quick charging response, followed by a lower charging current in the second stage for a steady and safe charging process.

In Case C, on the basis of Case B, a disturbance signal was added to the buck circuit's input voltage $U_{di}(i = 1,2,3,4)$. More specifically, a sharp decline of 800 V for 0.2 s was added to U_{di} at $t = 10$ s. The current-sharing curve plotted in **Fig. 6** illustrates the simulation results, which show that at $t = 10$ s, with disturbances, the current had a maximum decline of approximately 15 A, and then returned to the normal value within 0.6 s, which was

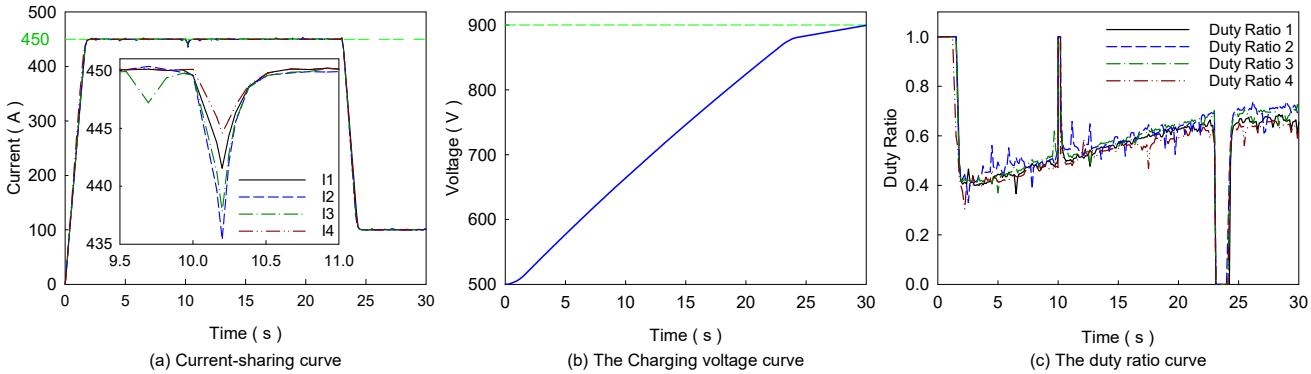

(a) Current-sharing curve (b) The Charging voltage curve (c) The duty ratio curve

Fig. 6. Current-sharing curve for Case C: on the basis of Case B, a disturbance signal is added at $t = 10$ s.

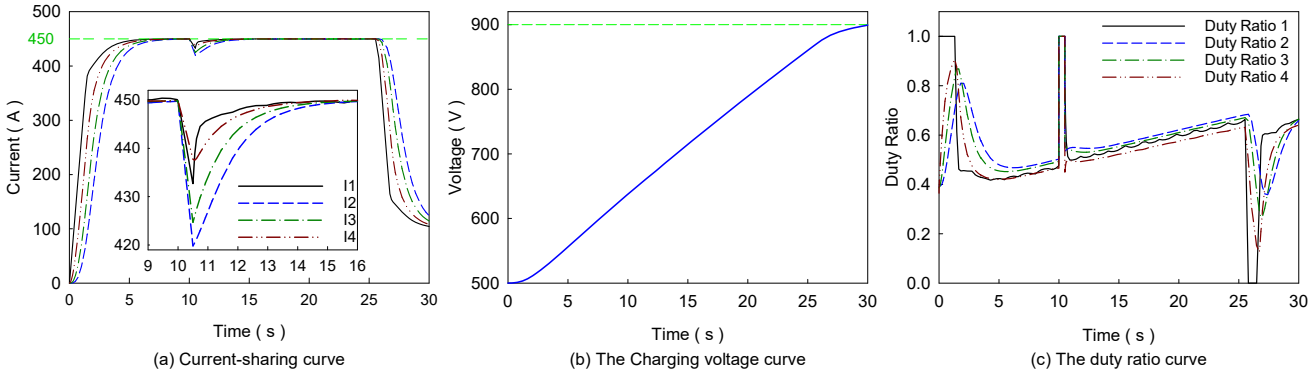

(a) Current-sharing curve (b) The Charging voltage curve (c) The duty ratio curve

Fig. 7. Current-sharing curve under traditional distributed control law: a comparison with Case C.

a quick response. **Fig. 6(b)** shows the charging voltage response, which exhibited almost no effects from the disturbances. The 800 V voltage drop was a very large disturbance, but the fluctuation of the charging current was relatively small. **Fig. 6(c)** shows the control output duty ratio curve. It maintained a constant maximum value before 2 s, which guaranteed a quick consensus. Then the duty ratio value kept increasing due to the rise in supercapacitor voltage. When $t = 10$ s, a sharp rise was regulated to counteract the voltage disturbance. When the voltage reached 900 V, the duty ratio dropped to 0 to decrease the charging current to 100 A. In short, we can conclude that the APF-based decentralized gradient control scheme can effectively reject the disturbances of the buck circuits, and thus perform current-sharing tasks.

Figure 7 shows a performance comparison using the traditional distributed control law depicted in [8] with Case C. All the parameter settings were the same, except for the controller. Obviously, the current convergence rate was slower than in Case C. Under disturbances at $t = 10$ s, the current had a maximum decline of about 30 A and recovered for 5 s, which was larger and longer than in **Fig. 6(a)**. Clearly, Case C rejected disturbances more efficiently. The curve in **Fig. 7(b)** also increased more slowly than in **Fig. 6(b)**, which indicated a slower response to the output voltage. The duty ratio curve depicted in **Fig. 7(c)**, which has a slow response to consensus as well as disturbance, also showed less competitive performance compared with **Fig. 6(c)**. Thus, we can conclude that the APF-based decentralized gradient control method performed better in terms of both convergence rate and disturbance rejection, making it a more effective and suitable way to achieve current sharing.

5. Conclusions

In this paper, a generalized APF-based decentralized gradient control was adopted to address the current imbalance problem for the parallel charging system of an energy storage-type light rail vehicle. A generalized potential function was employed to determine the interaction rule for the subchargers, converting the current-sharing problem into a problem of minimizing the potential function. A nonlinear decentralized gradient control law is proposed based on the gradient of the potential function. The boundedness of the control output was also considered with a general saturation function. The charging system proved to be cooperative stable. Simulations showed that the proposed current-sharing approach was effective and feasible, and had good performance in terms of both convergence rate and disturbance rejection.

Acknowledgements

The authors would like to acknowledge the National Natural Science Foundation of China (Grant No. 61379111, 61672537, 61672539, 61402538, 61403424, 61602529, 61502055, and 61503048) for their partial support of this work.

References:

[1] M. Camara, H. Gualous, F. Gustin, and A. Berthon, "Design and new control of dc/dc converters to share energy between supercapacitors and batteries in hybrid vehicles," IEEE Trans. on Vehicular Technology, Vol.57, No.5, pp. 2721-2735, 2008.

[2] H. Mao, L. B. Yao, C. S. Wang, and I. Batarseh, "Analysis of inductor current sharing in nonisolated and isolated multiphase dc–dc converters," IEEE Trans. on Industrial Electronics, Vol.54, No.6, pp. 3379-3388, 2007.

[3] K. Hwu and Y. Chen, "Current sharing control strategy based on phase link," IEEE Trans. on Industrial Electronics, Vol.59, No.2, pp. 701-713, 2012.

[4] B. Chen, Z. Huang, and R. Zhang, "Optimal Operation for Supercapacitor Storage System Using Piecewise LQR Voltage Equalization Control," J. Adv. Comput. Intell. Intell. Inform. (JACIII), Vol.20, No.2, pp. 317-323, 2016.

[5] K. De Brabandere, B. Bolsens, J. Van den Keybus, A. Woyte, J. Driesen, and R. Belmans, "A voltage and frequency droop control method for parallel inverters," IEEE Trans. on Power Electronics, Vol.22, No.4, pp. 1107-1115, 2007.

[6] S. K. Mazumder, M. Tahir, and K. Acharya, "Master–slave currentsharing control of a parallel dc–dc converter system over an rf communication interface," IEEE Trans. on Industrial Electronics, Vol.55, No.1, pp. 59-66, 2008.

[7] P. Li and B. Lehman, "A design method for paralleling current mode controlled dc-dc converters," IEEE Trans. on Power Electronics, Vol.19, No.3, pp. 748-756, 2004.

[8] J. G. Liu, Z. W. Huang, J. Wang, J. Peng, and W. R. Liu, "Distributed cooperative current-sharing control of parallel chargers using feedback linearization," Mathematical Problems in Engineering, Vol.2014, No.1, pp. 1-12, 2014.

[9] J. J. Sun, "Dynamic performance analyses of current sharing control for dc/dc converters," Ph.D. dissertation, Virginia Polytechnic Institute and State University, 2007.

[10] N. E. Leonard and E. Fiorelli, "Virtual leaders, artificial potentials and coordinated control of groups," Proc. of the 40th IEEE Conf. on Decision and Control, Vol.3, pp. 2968-2973, 2001.

[11] J. P. Desai, J. Ostrowski, and V. Kumar, "Controlling formations of multiple mobile robots," Proc. of IEEE Int. Conf. on Robotics and Automation, Vol.4, pp. 2864-2869, 1998.

[12] E. Rimon and D. E. Koditschek, "Exact robot navigation using artificial potential functions," IEEE Trans. on Robotics and Automation, Vol.8, No.5, pp. 501-518, 1992.

[13] L. Zubieta and R. Bonert, "Characterization of double-layer capacitors for power electronics applications," IEEE Trans. on Industry Applications, Vol.36, No.1, pp. 199-205, 2000.

[14] M. Li, C. K. Tse, H. H. Iu, and X. Ma, "Unified equivalent modeling for stability analysis of parallel-connected dc/dc converters," IEEE Trans. on Circuits and Systems II: Express Briefs, Vol.57, No.11, pp. 898-902, 2010.

[15] J. Abu-Qahouq, "Analysis and design of n-phase current-sharing autotuning controller," IEEE Trans. on Power Electronics, Vol.25, No.6, pp. 1641-1651, 2010.

[16] C. L. Zhang and R. Ordo nez, "Extremum-seeking control and applications: a numerical optimization-based approach," Springer Science & Business Media, 2011.

[17] J. Y. Yao, R. Ordonez, and V. Gazi, "Swarm tracking using artificial potentials and sliding mode control," J. of Dynamic Systems, Measurement, and Control, Vol.129, No.5, pp. 749-754, 2007.

[18] C. L. Zhang, A. Siranosian, and M. Krstic, "Extremum seeking for moderately unstable systems and for autonomous vehicle target tracking without position measurements," Automatica, Vol.43, No.10, pp. 1832-1839, 2007.

[19] S. Z. Khong, Y. Tan, C. Manzie, and D. Nesič, "Multi-agent source seeking via discrete-time extremum seeking control," Automatica, Vol.50, No.9, pp. 2312-2320, 2014.

[20] W. Ren, "Consensus tracking under directed interaction topologies: Algorithms and experiments," IEEE American Control Conf., pp. 742-747, 2008.

Name:
Hongtao Liao

Affiliation:
School of Information Science and Engineering, Central South University

Address:
Changsha, Hunan 410075, China

Brief Biographical History:

1994 Received the B.S. degree from Dalian Jiaotong University
2013 Received the M.S. degree from Southwest Jiaotong University
2014 Received the MBA degree from Central South University
2015- Ph.D. Student, School of Information Science and Engineering, Central South University

Main Works:

- Presiding over the research and development of the most advanced DC drive electric locomotive called SS9 in China.
- Achieving locomotive technical support and service of 20,000-ton heavy haul train traction on the Da-Qin rail line.
- Train control and cooperative control

Membership in Academic Societies:

- The Institute of Electrical and Electronics Engineers (IEEE)

Name:
Jun Peng

Affiliation:
Professor, School of Information Science and Engineering, Central South University

Address:
Changsha, Hunan 410075, China

Brief Biographical History:

1987 Received the B.S. degree from Xiangtan University
1990 Received the M.S. degree from National University of Defense Technology
2005 Received the Ph.D. degree from Central South University

Main Works:

- Cooperative control
- Cloud computing
- Wireless communications

Membership in Academic Societies:

- The Institute of Electrical and Electronics Engineers (IEEE)

Name:
Yanhui Zhou

Affiliation:
School of Information Science and Engineering, Central South University

Address:
Changsha, Hunan 410075, China

Brief Biographical History:
2006-2010 Bachelor of Engineering, School of Information and Electrical Engineering, Hunan University of Science and Technology
2011-2014 M.D. Student, School of Information Science and Engineering, Central South University
2014- Ph.D. Student, School of Information Science and Engineering, Central South University

Main Works:
- New energy and renewable energy
- Power electronics
- Disturbance rejection control

Name:
Zhiwu Huang

Affiliation:
Professor, School of Information Science and Engineering, Central South University

Address:
Changsha, Hunan 410075, China

Brief Biographical History:
1983-1987 B.S. degree from Xiangtan University
1987-1989 M.S. degree in Industrial Automation from Department of Automatic Control, University of Science and Technology Beijing
2002-2006 Ph.D. degree from Central South University

Main Works:
- Fault diagnostic technique
- Cooperative control

Membership in Academic Societies:
- The Institute of Electrical and Electronics Engineers (IEEE)

Name:
Feng Zhou

Affiliation:
School of Information Science and Engineering, Central South University

Address:
Changsha, Hunan 410075, China

Brief Biographical History:
2007-2011 Bachelor of Engineering, School of Information Science and Engineering, Central South University
2011-2013 M.D. Student, School of Information Science and Engineering, Central South University
2013- Ph.D. Student, School of Information Science and Engineering, Central South University

Main Works:
- Cooperative control
- Multi-agent systems